Supporting Information

The First Step in Catalysis of the Radical *S*-Adenosylmethionine Methylthiotransferase MiaB Yields an Intermediate with a [3Fe-4S]^{0}-like Auxiliary Cluster

Bo Zhang,[1,†] Arthur J. Arcinas,[2,§] Matthew I. Radle,[1] Alexey Silakov,[1] Squire J. Booker,[1,2,3,] and Carsten Krebs[1,2,*]*

[1]Department of Chemistry, [2]Department of Biochemistry and Molecular Biology, and [3]Howard Hughes Medical Institute, The Pennsylvania State University, University Park, Pennsylvania 16802, United States

Table of Contents

Materials and Methods

Materials

DNA-modifying enzymes and reagents were obtained from New England Biolabs (Ipswich, MA). FastAP alkaline phosphatase was obtained from ThermoScientific. P1 nuclease was obtained from US Biologicals (Salem, MA). Sodium methanethiolate and phosphodiesterase from *Crotalus adamanteus* were obtained from Sigma (St. Louis, MO). Egg white lysozyme and deoxyribonuclease were purchased from Alfa Aesar (Ward Hill, MA). Expression plasmids pET28a and pET26b were obtained from EMD Millipore, and DH5α and BL21(DE3) strains were obtained from Invitrogen (Carlsbad, CA). *Escherichia coli miaA,* used to generate the i^6A tRNA substrate, was PCR amplified, expressed and purified as previously described.[1]

Cloning and overexpressing of *Bt* MiaB and variants

The *Bacteroides thetaiotaomicron* (*Bt*) *miaB* gene (NCBI accession NP_812107.1) was amplified from a pSGC-His construct (obtained from Steve Almo (Albert Einstein University) of the Enzyme Function Initiative using the polymerase chain reaction (PCR). It was cloned into a pET28a expression vector, which was used to co-transform *Ec* BL21(DE3) along with pDB1282 for over production, as previously described.[2,3] Plasmid pDB1282 encodes *Azotobacter vinelandii* proteins involved in Fe/S cluster assembly and trafficking, and enhances the over production of Fe/S proteins in a soluble form.

Site-directed mutagenesis was conducted using the QuikChange II system (Agilent, Santa Clara, CA) in conjunction with the *Bt* MiaB–pET28a construct as template and the mutagenesis primers described below. The *Bt* MiaB Cys to Ala variant to the RS cluster cysteinyl ligands (C170A, C174A, C177A) for the $^{\Delta RS}$MiaB variant was generated using the forward (5'- CC ATC ATG CGC GGA GCC AAT AAC TTC GCC ACC TAC GCT ATC GTG CCT TAT ACA CG -3') and reverse (5'- CG TGT ATA AGG CAC GAT AGC GTA GGT GGC GAA GTT ATT GGC TCC GCG CAT GAT GG -3') mutagenesis primers. The *Bt* MiaB Cys to Ala variants of the auxiliary cluster cysteinyl ligands (C26A, C62A, C96A) for the $^{\Delta Aux}$MiaB variant was generated sequentially. The C26A variant was generated using the forward (5'- C GAG ACT TAT GGC GCC CAG ATG AAC GTG G -3') and reverse (5'- C CAC GTT CAT CTG GGC GCC ATA AGT CTC G -3') primers. The C62A variant was generated using the forward (5'- GCA GTG TTT ATG AAT ACC GCC TCT ATC CGT GAC AAT GC -3') and reverse (5'- GC

ATT GTC ACG GAT AGA GGC GGT ATT CAT AAA CAC TGC -3') primers. The C96A variant was generated using the forward (5'- C GTA CTG GGC GCT ATG GCG GAA CG -3') and reverse (5'- CG TTC CGC CAT AGC GCC CAG TAC G -3') primers. After PCR mutagenesis, the resulting constructs were digested with DpnI for 3 h at 37 ˚C prior to transformation into DH5□ using standard molecular biological techniques and subsequent nucleic acid sequence. The constructs bearing the correct sequence were co-transformed with the plasmid pDB1282 into the BL21(DE3) expression strain for overproduction.

Expression and Purification of *Bt* MiaB

The overproduction of *Bt* MiaB and variants was conducted in 16 L of M9 minimal media supplemented with 25 μM $^{57}FeCl_3$ upon inoculation and shaken at 180 rpm at 37 °C. At an OD600 of 0.3, L-(+)-arabinose was added to a concentration of 0.2% (w/v) with 300μM L-cysteine and 50 μM $^{57}FeCl_3$. At an OD600 of 0.6, the flasks were cooled prior to addition of 200 μM IPTG and incubation at 18 °C for 16 h. Afterwards, cell paste was collected by centrifugation at 6,000 × *g* for 15 min at 4 °C. Purification of *Bt* MiaB was conducted within an anaerobic chamber (Coy, Grass Lakes, MI) maintained in N_2 and H_2 (95%/5%) with less than 1 ppm O_2 using a palladium catalyst. Frozen cell paste was thawed in lysis buffer (50 mM HEPES pH 7.5, 300 mM KCl, 10 mM imidazole, 10 mM β-mercaptoethanol, 10 mM $MgCl_2$, 1 mg/ml lysozyme, 0.5 mg/ml DNase, 0.5 mg/ml PMSF). The cells were disrupted by sonication and the crude lysate was clarified by centrifugation at 40,000 × *g* for 1.5 h at 4 °C. The clarified lysate was loaded onto Ni-NTA resin, washed with 150 mL of wash buffer (lysis buffer with 20 mM imidazole and without lysozyme, DNase and PMSF), then eluted with elution buffer (wash buffer with 250 mM imidazole). During elution, the dark brown fractions containing protein were pooled and buffer exchanged into gel filtration buffer (50 mM HEPES pH 7.5, 300 mM KCl, 1 mM DTT, 10 mM $MgCl_2$, 30 % (v/v) glycerol). The as-isolated *Bt* MiaB was subjected to FPLC size exclusion chromatography using a sephadex S200 16/60. Chemical reconstitution of the *Bt* MiaB Fe-S clusters was conducted as previously described for MiaB from *Thermotoga maritima.*[1]

Preparation of MiaB tRNA substrate

The full–length i^6A $tRNA^{Phe}$substrate was generated using *in vitro* run-off transcription with T7

RNA polymerase using a DNA template containing a T7 promoter region followed by the nucleic acid sequence corresponding to *Tm* $tRNA^{Phe}$. To generate the template, a forward (5′ – AAT TCC TGC AGT AAT ACG ACT CAC TAT AGG CCA GGT AGC TCA GTT GGT AGA GCA CTG G – 3′) and reverse (5′ – TmGG CCA GGG GCG GAA TCG AAC CGC CGA CAC CTG GAT TTT CAG TCC AGT GCT CTA CC – 3′) primer containing a T7 promoter, a complementary sequence (underlined) and 2′-O-methyldeoxyguanosine (mG) were used in multiple PCR samples (10 × 100 µL) for primer overlap extension. The resulting product was purified by agarose gel electrophoresis, ethanol precipitated, and resuspended in water. The template was used at a final concentration of 2 µg/µL within *in vitro* transcription reactions containing 40 mM Tris-HCl pH 8, 10 mM DTT, 25 mM $MgCl_2$, 4 mM each of NTPs, and 10 % (v/v) of 51 µM T7 RNA polymerase. Transcription reactions were incubated at 37 ℃ for 3 h, centrifuged at 8,000 × *g* for 10 min, and the supernatant retained. Afterwards, 50 mM EDTA pH 8 was added, and the solution was concentrated to approximately 2.5 mL using an Amicon Ultra centrifugal filter with a 3 kDa NMWL cutoff. The RNA was extracted twice with (25:24:1) phenol:chloroform:isoamyl alcohol and the RNA was ethanol precipitated from the aqueous fraction overnight. The reaction was centrifuged, and the pellet was resuspended in sterile RNAse-free H_2O. The installation of the isopentenyl group at N6 of adenosine 37 in the tRNA was performed using *E. coli* MiaA according to previously published procedures[1].

Preparation of MiaB samples for Mössbauer, EPR and LC/MS analysis

Bt MiaB samples prepared for coupled Mössbauer, EPR and LC/MS analysis contained 165 µM (RC) WT *Bt* MiaB in buffer system (50 mM HEPES pH 7.5, 300 mM KCl and 10 mM $MgCl_2$) in a total volume of 505 µL, of which 150 µL was prepared for EPR analysis of non-reduced protein (**Figure S1A**), 150 µL was reduced with 2 mM dithionite for EPR analysis of reduced protein (**Figure S1B**), and 200 µL was prepared for Mössbauer analysis of non-reduced protein. Methylated *Bt* MiaB samples contained 165 µM WT enzyme and 330 µM i^6A $tRNA^{Phe}$ in buffer system as described above and initiated by addition of 600 µM SAM at 30 ˚C in a total volume of 455 µL. Of the total volume, 100 µL was utilized for LC/MS analysis during the course of the methylation reaction, during which 10 µL aliquots of the sample mixture was quenched in 0.2 M H_2SO_4, and prepared for LC/MS analysis as described above (**Figure 1A**). After 20 min of the methylation reaction, 150 µL of the reaction mixture was prepared for EPR analysis (**Figure S1C**), and 200 µL was prepared for Mössbauer analysis. Reaction conditions for *Bt* MiaB under turnover conditions were identical to the methylation conditions described

above and incubated for 20 min at 30 ˚C prior to reaction initiation with 2 mM dithionite in a total volume of 455 µL. Of the total volume, 100 µL was utilized for LC/MS analysis during the course of the reaction, during which 10 µL aliquots of the methylation reaction was quenched in 0.2M H_2SO_4, and prepared for LC/MS analysis as described above (**Figure 1B**). After 15 min of reaction initiation, 150 µL of the reaction mixture was prepared for EPR analysis (**Figure S1D),** and 200 µL was prepared for Mössbauer analysis.

Bt MiaB samples prepared for coupled Mössbauer and LC/MS analysis contained either 200 µM enzyme (for MiaB WT), or 300 µM enzyme (for $^{\Delta RS}$MiaB and, $^{\Delta Aux}$MiaB), prepared in the buffer system described above in a total volume of 450 µL. Samples incubated with substrate additionally contained either 200 µM i^{6}A tRNA^{Phe} (MiaB WT, $^{\Delta RS}$MiaB) or 320 µM i^{6}A tRNA^{Phe} ($^{\Delta Aux}$MiaB) in a total volume of 450 µL and incubated for 15 min at 30 ˚C prior to Mössbauer analysis. Samples prepared under methylation conditions additionally contained either 500 µM SAM (MiaB WT, $^{\Delta RS}$MiaB) or 600 µM SAM ($^{\Delta Aux}$MiaB), in a total volume of 550 µL and were incubated for 1 h at 30 ˚C prior to utilizing 100 µL for LC/MS monitoring and the remainder for Mössbauer analysis. Samples methylated under reducing conditions (MiaB WT) additionally contained 1 mM SAM and 1 mM dithionite in a total volume of 550 µL, and were incubated at 30 ˚C for 1 h prior to Mössbauer analysis. Assays incubated with methanethiol contained 200 µM of MiaB and 1 mM CH_3SH in a total volume of 550 µL and incubated for 30 min at 30 ˚C prior Mössbauer analysis.

^{57}Fe Mössbauer spectroscopy

The Mössbauer spectra were recorded at 4.2 K on constant acceleration spectrometers equipped with a Janis SVT-400 variable-temperature cryostat (zero and 53 mT) or 8TMOSS-OM-12SVT variable-temperature cryostat (up to 8 T). The external magnetic field was applied parallel to the γ beam. All isomer shifts quoted are relative to the centroid of the spectrum of α-iron metal at room temperature. Simulations were carried out using the WMOSS spectral analysis software from SEECO (www.wmoss.org; Edina, MN). Analyses of the MiaB [3Fe-4S]^0-like cluster are based on spin-Hamiltonian formalism (Equation 1), in which the first three terms represent the electron Zeeman effect and zero field splitting (ZFS) of the electron-spin ground state, the fourth term represents the interaction between the electric field gradient and the nuclear quadrupole moment, the fifth term describes the magnetic hyperfine interactions of the electronic spin with the ^{57}Fe nucleus, and the last term represents the ^{57}Fe nuclear Zeeman interaction. The electronic spin *S* in the equation refer to the total spin of the [3Fe-4S]^0-like cluster. Simulations were carried out with respect to the total electron spin of the [3Fe-4S]^0-like cluster and in the slow relaxation limit. All symbols have their usual meanings.

$$\mathbf{H} = \beta \mathbf{S} \cdot \mathbf{g} \cdot \mathbf{B} + D\left(\mathbf{S}_z^2 - \frac{S(S+1)}{3}\right) + E\left(\mathbf{S}_x^2 - \mathbf{S}_y^2\right) + \sum_{i=1}^{3} \frac{eQV_{zz,i}}{4}\left[\mathbf{I}_{z,i}^2 - \frac{I_i(I_i+1)}{3} + \frac{\eta}{3}\left(\mathbf{I}_{x,i}^2 - \mathbf{I}_{y,i}^2\right)\right] + \sum_{i=1}^{3} \mathbf{S} \cdot \mathbf{A}_i \cdot \mathbf{I}_i - \sum_{i=1}^{3} g_n \beta_n \mathbf{B} \cdot \mathbf{I}_i$$

(Equation 1)

The number of adjustable parameters for the spin Hamiltonian analysis is large. For each electronic spin ground state, in addition to the two zero-field splitting (ZFS) parameters (*D* and *E/D*), there are 14 parameters for each of the three individual Fe site (isomer shift; quadrupole splitting; the asymmetry parameter, η; three Euler angles that correlate the electric field gradient (EFG) tensors and the frame of the ZFS tensors; three principle components of the magnetic hyperfine **A** tensor; three Euler angles that rotate the **A** and EFG tensors into the frame of the ZFS tensor; the line width; and absorption area). In order to simplify the Mössbauer analysis of the MiaB [3Fe-4S]^0-like cluster to extract the most relevant spectroscopic information, the two sets of Euler angles were fixed to zero, and the line width and absorption area were constrained to be equal for the three sites.

EPR spectroscopy

Continuous wave X-band EPR spectra were obtained using a Bruker Elexsys E-560 spectrometer (Billerica, MA) equipped with a SuperX FT microwave bridge, an ITC503S temperature controller and ESR900 helium cryostat from Oxford Instruments (Concord, MA). Samples were analyzed at 10–15 K with 20 dB microwave power, 10 G modulation amplitude, 9.48 GHz microwave frequency and a receiver gain setting of $1x10^5$. Spin quantification of spectral features were determined by double integration and comparison of the signal area to that of a 200 μM Cu^{2+}-EDTA standard solution, utilizing Kazan Viewer (Alexey Silakov, University Park, PA) and MatLab (Mathworks, Natick, MA) software for data analysis.

Mössbauer-spectroscopic characterization of wild-type *Bt* MiaB, and $^{\Delta Aux}$MiaB and $^{\Delta RS}$MiaB variants.

To facilitate the analysis of the Mössbauer spectra of wild-type (wt) *Bt* MiaB, spectra of variants lacking either auxiliary cluster ($^{\Delta Aux}$MiaB) or radical SAM cluster ($^{\Delta RS}$MiaB) were recorded.

The 4.2-K/53-mT spectrum of reconstituted $^{\Delta Aux}$MiaB sample, which contains only the RS cluster, revealed an asymmetric doublet with a noticeably broader and partially resolved high-energy line (**Figure S2A**). The spectral features are reminiscent of those of the SAM-bound $[4Fe\text{-}4S]^{2+}$ clusters, in which coordination of SAM to the non-cysteinyl-ligated Fe leads to increased site differentiation.[4,5] Since no SAM was added during sample preparation, it is possible that the observed site-differentiation of the radical SAM cluster is caused by coordination of an exogenous molecule to the unique Fe-site.[6] The spectrum can be adequately simulated as summation of three quadrupole doublets with the following parameters: δ = 0.45 mm/s, $|\Delta E_Q|$ = 1.07 mm/s and $\Gamma_{L,R}$ = 0.40 mm/s for the valence-delocalized pair (50% of total ^{57}Fe absorption), δ = 0.67 mm/s, $|\Delta E_Q|$ = 1.28 mm/s, and $\Gamma_{L,R}$ = 0.31 mm/s for the Fe^{2+} site of the partially valence-trapped pair (25% of total ^{57}Fe absorption), and δ = 0.36 mm/s, $|\Delta E_Q|$ = 1.04 mm/s, and $\Gamma_{L,R}$ = 0.28 mm/s for the Fe^{3+} site of the partially valence-trapped pair (25% of total ^{57}Fe absorption).

The 4.2-K/53-mT spectrum (**Figure S2B**) associated with the Aux cluster from the $^{\Delta RS}$MiaB sample can be analyzed as a broad, slightly asymmetric quadrupole doublet with parameters characteristic for $[4Fe\text{-}4S]^{2+}$ clusters with two valence-delocalized pairs (δ = 0.45 mm/s, $|\Delta E_Q|$ = 1.10 mm/s, Γ_L = 0.32 mm/s and Γ_R = 0.35 mm/s (93% of total ^{57}Fe absorption). The spectrum also revealed the presence of a weak absorption at ~0.5 mm/s, which indicates a small amount of $[2Fe\text{-}2S]^{2+}$ cluster in the sample (δ = 0.30 mm/s, $|\Delta E_Q|$ = 0.48 mm/s, and $\Gamma_{L,R}$ = 0.30 mm/s, accounting for 7 % of total ^{57}Fe absorption).

Subsequently, as shown in **Figure S2C**, the 4.2-K/53-mT spectrum of the wt *Bt* MiaB (165 μM enzyme, 7.56 Fe/MiaB) can be simulated as weighted superposition of the partially valence-trapped RS $[4Fe\text{-}4S]^{2+}$ cluster (45% of total ^{57}Fe), the valence-delocalized Aux $[4Fe\text{-}4S]^{2+}$ cluster (43% of total ^{57}Fe), and a small amount of $[2Fe\text{-}2S]^{2+}$ cluster (12% of total ^{57}Fe). On the basis of Fe and protein quantification, the Mössbauer analysis revealed that the samples contain 0.85 RS $[4Fe\text{-}4S]^{2+}$ cluster, 0.81 Aux $[4Fe\text{-}4S]^{2+}$ cluster, 0.45 $[2Fe\text{-}2S]^{2+}$ cluster. Additionally, EPR

characterization of an identical sample revealed the presence of trace amount of cuboidal [3Fe-4S]$^{+}$ cluster (6.7 μM cluster, less than 0.04 cluster per MiaB monomer).

The 4.2-K/zero-field spectrum of wt *Bt* MiaB reacted with SAM (**Figure S3**) was analyzed as a superposition of the various components. Importantly, the spectrum reveals a pronounced shoulder at ~+1.6 mm/s, which does not emanate from the [3Fe-4S]^{0}-like cluster. This shoulder is distinct from the shoulder at ~+1.3 mm/s in the spectrum of $^{\Delta Aux}$MiaB (**Figure S2A**). This shoulder is at a position typical of the high-energy line of the unique Fe site of the RS [4Fe-4S]$^{2+}$ cluster that is coordinated by an exogenous molecule (e.g. SAM, TRIS buffer). We tentatively attribute it to coordination of *S*-adenosylhomocysteine to the unique Fe site. Because this shoulder accounts for 6-7% of total intensity, there is ~25% of total intensity attributable to this cluster. The various spectral components include those of the [3Fe-4S]^{0}-like cluster (red line, simulated using parameters quoted in the main text, 30% total intensity); the high-spin Fe^{II} species (green line, δ = 1.32 mm/s, ΔE_Q = 2.82 mm/s, 12% total intensity); fully valence-delocalized [4Fe-4S]$^{2+}$ cluster (orange line, δ = 0.44 mm/s, ΔE_Q = 1.12 mm/s, 22% total intensity); and site-differentiated [4Fe-4S]$^{2+}$ cluster (blue line, δ_1 = 0.44 mm/s, ΔE_{Q1} = 1.12 mm/s, 13% total intensity; δ_2 = 0.37 mm/s, ΔE_{Q2} = 0.81 mm/s, 6.5% total ^{57}Fe absorption; δ_3 = 0.73 mm/s, ΔE_{Q3} = 1.68 mm/s, 6.5% total intensity); and [2Fe-2S]$^{2+}$ cluster (purple line, δ = 0.29 mm/s, ΔE_Q = 0.50 mm/s, 4% total intensity).

Evaluation of alternative spin states as ground state of the [3Fe-4S]^0-like cluster.

We start our exploration of possible spin ground states using the model introduced by Papaefthymiou, *et al.*, developed for the [3Fe-4S]^0 cluster from *Desulfovibrio gigas* ferredoxin.[7]

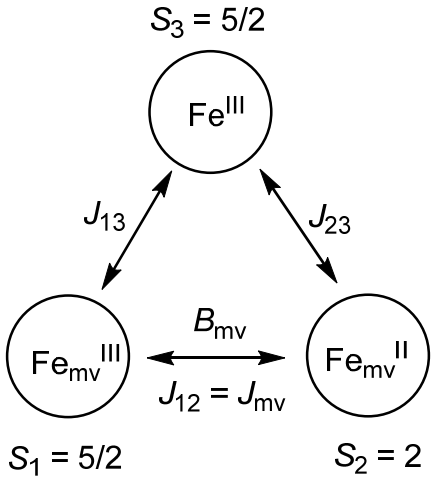

This spin coupling model invokes in the first step the coupling of the spins of the formally high-spin (HS) Fe^{III}, $\mathbf{S}_1$ = 5/2, and HS Fe^{II} sites, $\mathbf{S}_2$ = 2, comprising the mixed-valent (MV) unit, yielding $\mathbf{S}_{mv}$ [= $\mathbf{S}_{12}$], and in the second step coupling of $\mathbf{S}_{mv}$ with the spin of the HS Fe^{III} site, $\mathbf{S}_3$ = 5/2, to yield the total spin, $\mathbf{S}_{tot}$. Spin states are denoted in the following as $|S_{mv}, S_{tot}\rangle$. This model requires three Heisenberg exchange coupling constants, J_{12}, J_{13}, and J_{23}. The simplest assumption invokes three identical J-values, which is justified by the approximately three-fold symmetry of the cluster. These interactions are described by the first term in equation S1. In addition, the model assumes the double exchange interaction, also known as spin-dependent delocalization, between the two Fe ions of the MV unit, which is parameterized by the second term in equation S1 with the double exchange parameter, B_{mv}. This term lifts the two-fold degeneracy of the spin states, which is due to the fact that in symmetric MV compounds, two isoenergetic resonance structures exist, *viz* $M_A^{n+}\cdots M_B^{(n+1)+}$ and $M_A^{(n+1)+}\cdots M_B^{n+}$.

$$E(S_{tot}, S_{mv}) = 1/2\, J\, [S_{tot} \cdot (S_{tot} + 1)] \;\pm\; B_{mv}\, (S_{mv} + 1/2) \qquad \text{(S1)}$$

The dependence of the relative energies of the various spin states ($E(S_{tot}, S_{mv})/J$) as a function of B_{mv}/J (equation S2) can be plotted to determine the possible spin ground states (**Figure S15A**, also shown in **Figure 7** from Papaefthymiou, *et al.* [7]).

$$E(S_{tot}, S_{mv})/J = 1/2\ [S_{tot} \cdot (S_{tot} + 1)] \quad \pm \quad B_{mv}/J\ (S_{mv} + 1/2) \qquad \text{(S2)}$$

The three possible ground states are $|5/2\ ,0\rangle$ for B_{mv}/J between 0 and 1, $|7/2\ ,1\rangle$ for B_{mv}/J between 1 and 2, and $|9/2\ ,2\rangle$ for $B_{mv}/J > 2$. For the $[3Fe\text{-}4S]^0$ clusters, the $|9/2\ ,2\rangle$ state is the ground state because the large value of B_{mv} favors the parallel alignment of the core spins of the MV unit to give $S_{mv} = 9/2$, which is antiferromagnetically (AF) coupled with the Fe^{III} site to give $S_{tot} = 2$.

In the next step we assumed that one J-value is different from the other two (equal) J-values. The first case we consider invokes that J_{mv} is different from $J_{13} = J_{23}$ [$= J$]. For such a system, the expression of the energies is given by equation S3 as:

$$\begin{aligned} E(S_{tot}, S_{mv}) = 1/2\ J_{mv}\ [S_{mv} \cdot (S_{mv} + 1)] + \quad & 1/2\ J\ [S_{tot} \cdot (S_{tot} + 1) - S_{mv} \cdot (S_{mv} + 1)] \\ \pm \quad & B_{mv}\ (S_{mv} + 1/2) \end{aligned} \qquad \text{(S3)}$$

The first two terms describe the contribution from the Heisenberg exchange, while the second term describes the double exchange interaction of the MV pair. Again, the dependence of $E(S_{tot}, S_{mv})/J$ as a function of B_{mv}/J (equation S4) can be plotted for for various ratios J_{mv}/J to evaluate the effect of non-identical J-values (**Figure S15B-E** for $J_{mv}/J = 0.75$, 0.5, 2, and 3, respectively).

$$\begin{aligned} E(S_{tot}, S_{mv})/J = 1/2\ J_{mv}/J\ [S_{mv} \cdot (S_{mv} + 1)] \quad + \quad & 1/2\ [S_{tot} \cdot (S_{tot} + 1) - S_{mv} \cdot (S_{mv} + 1)] \\ \pm \quad & B_{mv}/J\ (S_{mv} + 1/2) \end{aligned} \qquad \text{(S4)}$$

We show as **Figure 5** of the main manuscript the areas of the five possible ground states as a function of J_{mv}/J vs B_{mv}/J.

The case $J_{mv}/J < 1$ (i.e. $J_{mv} < J$) leads to progressive lowering of the relative energy of the $|9/2\ ,2\rangle$ state. For $J_{mv}/J = 0.75$, this state is the ground state for $B_{mv}/J > 0.875$ (**Figure S15B**) and for $J_{mv}/J = 0.5$, this state is the ground state for any value of B_{mv}/J (**Figure S15C**). The behavior can be understood in terms of the forces that lead to stabilization of either the parallel or antiparallel alignment of the spins of the MV unit. AF coupling within the MV unit favors antiparallel alignment of the spins within the MV unit. By contrast, the AF couplings between the Fe^{III} site

and the two sites of the MV unit, as well as the double exchange interaction within the MV unit both will favor the parallel alignment of the spins within the MV unit. In the limiting case for $B_{mv}/J = 0$ (this is the y-axis of **Figure S15C**) and $J_{mv}/J \leq 0.555$ (5/9), the $|9/2\ ,2\rangle$ state is the ground state, because the stronger AF interactions with the Fe^{III} site force the spins of the MV unit to be parallel.

Conversely, for $J_{mv}/J > 1$ the trend reverses, because now states with lower S_{mv} are lowered in energy. For $J_{mv}/J = 2$ (**Figure S15D**) the $|3/2\ ,1\rangle$ state becomes the ground state for $B_{mv}/J < 1.5$ and for $J_{mv}/J = 3$ (**Figure S15E**) the $|1/2\ ,2\rangle$ state even becomes the ground state for $B_{mv}/J < 1$.

The second case we consider invokes that one of the J-values between the ferric site and one of the Fe ions of the MV unit is different, while the other two J-values are the same, e.g. $J_{23} \neq J_{12} = J_{13}$. This case is more difficult to evaluate, because there is no simple analytical solution for the energies of the various spin states, if the same spin coupling model is used ($\mathbf{S}_1 + \mathbf{S}_2 = \mathbf{S}_{mv}$; $\mathbf{S}_{mv} + \mathbf{S}_3 = \mathbf{S}_{tot}$). Therefore, we treat this case qualitatively. Compared to the case with three identical J-values, the increase (decrease) of the J_{23} leads to a stabilization (destabilization) of states with parallel alignment of $\mathbf{S}_1$ and $\mathbf{S}_2$ to $\mathbf{S}_{mv} = 9/2$, because of the stronger (weaker) AF coupling between sites 2 and 3. Thus, the effect of changing the ratio J_{23}/J is opposite to that of changing J_{mv}/J (see above).

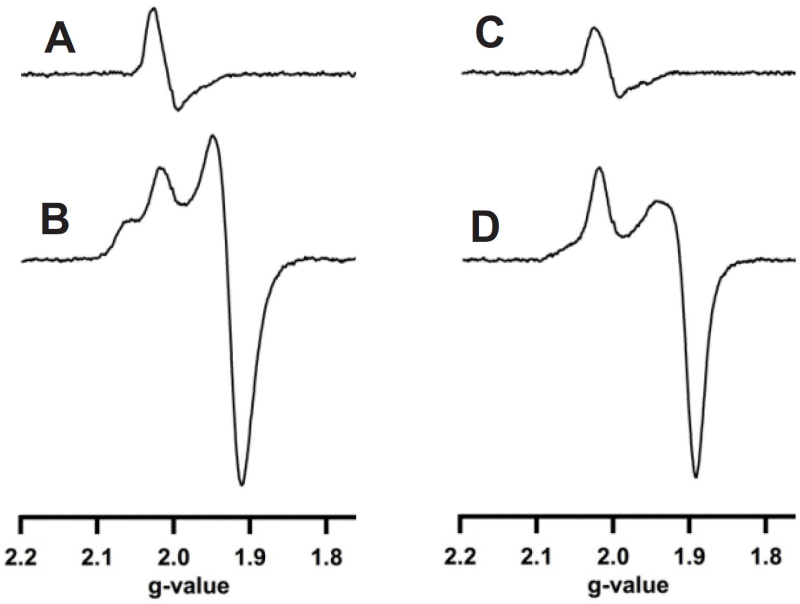

Figure S1. EPR analysis of various samples of reconstituted, wild-type *Bt* MiaB. Spectra were obtained at 15 K, with 0.2 mW microwave power, 9.623 GHz microwave frequency, 0.1 mT modulation amplitude, and 39 ms conversion time. (**A**) The spectrum obtained from a sample of 165 μM MiaB in the absence of reductant indicates the presence of an EPR active $[3Fe–4S]^{1+}$ cluster in RCN MiaB. (**B**) After reduction with dithionite (400 μM), reduced $[4Fe–4S]^{1+}$ clusters with parameters g = 2.08 and 2.02 were observed in MiaB WT, with the feature at g = 2.08 corresponding to the Aux cluster of the enzyme. (**C**) After incubation of MiaB with two equivalents (330 μM) of i^6A tRNA and excess SAM (600 μM) for 20 min in the absence of reductant, an EPR signal consistent with a $[3Fe–4S]^{1+}$ cluster was observed. (**D**) Under turnover conditions in the presence of i^6A tRNA (330 μM), excess SAM (600 μM) and dithionite (2 mM), the Aux cluster feature (g = 2.08) is less visible in comparison to the reduced enzyme alone.

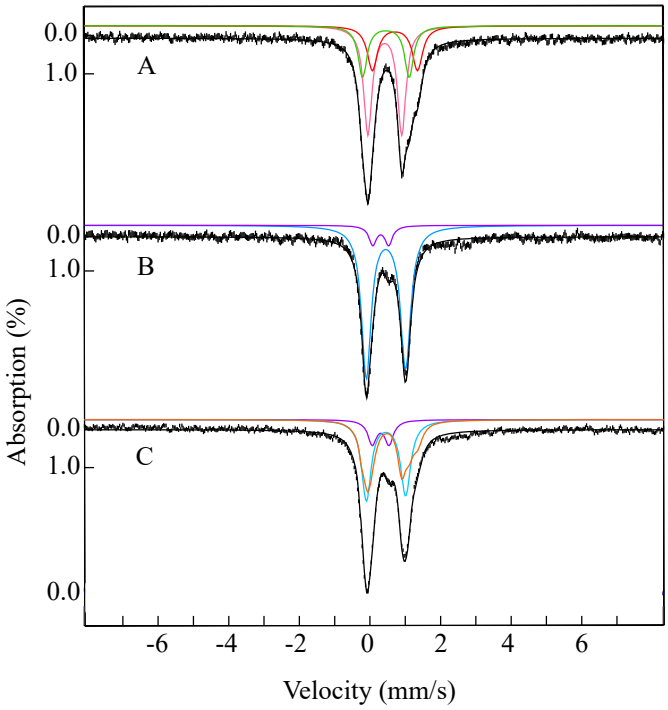

Figure S2. 4.2 K Mössbauer spectra of $^{\Delta Aux}$MiaB (A), $^{\Delta RS}$MiaB (B) and wt *Bt* MiaB (C&D). Unless otherwise specified, all spectra were recorded in an external magnetic field of 53 mT applied parallel to the γ beam. (**A**) The spectrum of $^{\Delta Aux}$MiaB is shown as vertical bars. The spectrum can be simulated with the following parameters: δ = 0.45 mm/s, ΔE_Q = 1.07 mm/s and $\Gamma_{L,R}$ = 0.40 mm/s for the valence-delocalized pair (50% of total absorption, magenta line), δ = 0.67 mm/s, ΔE_Q = 1.28 mm/s, and $\Gamma_{L,R}$ = 0.31 mm/s for the Fe^{II} site of the partially valence-trapped pair (25% of total Fe absorption, red line), and δ = 0.36 mm/s, $|\Delta E_Q|$ = 1.04 mm/s, and $\Gamma_{L,R}$ = 0.28 mm/s for the Fe^{III} site of the partially valence-trapped pair (25% of total absorption, green line). The added contribution is shown as black line. (**B**) The spectrum of $^{\Delta RS}$MiaB is shown as vertical bars. The light blue and purple lines are quadrupole doublet simulations of the Aux $[4Fe\text{-}4S]^{2+}$ cluster (δ = 0.45 mm/s, ΔE_Q = 1.10 mm/s, Γ_L = 0.32 mm/s and Γ_R = 0.35 mm/s, 93% of total absorption) and the $[2Fe\text{-}2S]^{2+}$ cluster (δ = 0.30 mm/s, ΔE_Q = 0.48 mm/s, and $\Gamma_{L,R}$ = 0.30 mm/s, 7 % of total absorption), respectively. The added contribution is shown as black line. (**C**) The spectrum of wt *Bt* MiaB (vertical bars). The orange, light blue, and purple lines mark the spectral contributions from the RS $[4Fe\text{-}4S]^{2+}$ cluster with the above parameters (45% of total intensity) the Aux $[4Fe\text{-}4S]^{2+}$ cluster with the above parameters (43% of total intensity), and the $[2Fe\text{-}2S]^{2+}$ cluster with the above parameters (12% of total intensity), respectively. The added contribution is shown as black line.

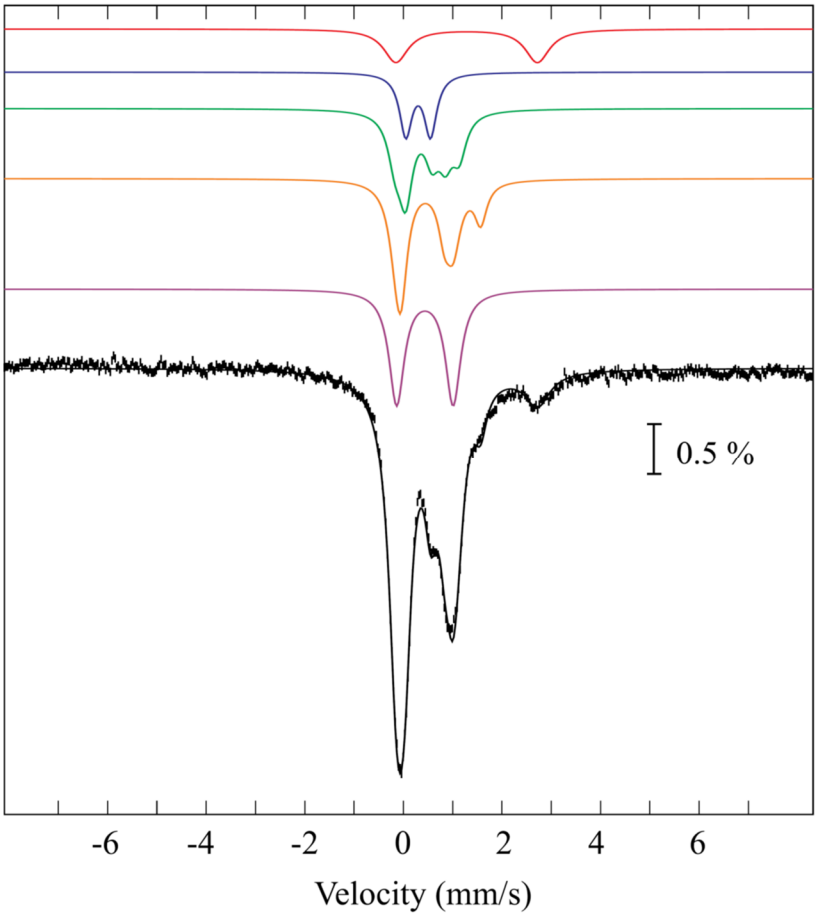

Figure S3. Analysis of the 4.2 K/zero-field Mössbauer spectrum of *Bt* MiaB after incubation with tRNA and SAM for 20 min. The spectrum is the same as the one presented in main text Figure 2B. The experimental data is shown as vertical bars and the simulation is shown as black line. The simulated spectral contributions from individual components are as the following: the high-spin Fe^{II} species (red line, δ = 1.28 mm/s, ΔE_Q = 2.87 mm/s, 12% total intensity); $[2Fe\text{-}2S]^{2+}$ cluster (blue line, δ = 0.30 mm/s, ΔE_Q = 0.50 mm/s, 12% total intensity); $[3Fe\text{-}4S]^{0}$-like cluster (green line, δ = 0.31 mm/s, ΔE_Q = 0.58 mm/s, δ = 0.35 mm/s, ΔE_Q = 1.02mm/s, δ = 0.61 mm/s, ΔE_Q = 1.04 mm/s, 9% each of total intensity); site-differentiated $[4Fe\text{-}4S]^{2+}$ cluster (orange line, δ_1 = 0.43 mm/s, ΔE_{Q1} = 1.14 mm/s, 13% total intensity; δ_2 = 0.38 mm/s, ΔE_{Q2} = 0.87 mm/s, 6.5% total ^{57}Fe absorption; δ_3 = 0.77 mm/s, ΔE_{Q3} = 1.61 mm/s, 6.5% total intensity); and fully valence-delocalized $[4Fe\text{-}4S]^{2+}$ cluster (purple line, δ = 0.43 mm/s, ΔE_Q = 1.14 mm/s, 27% total intensity).

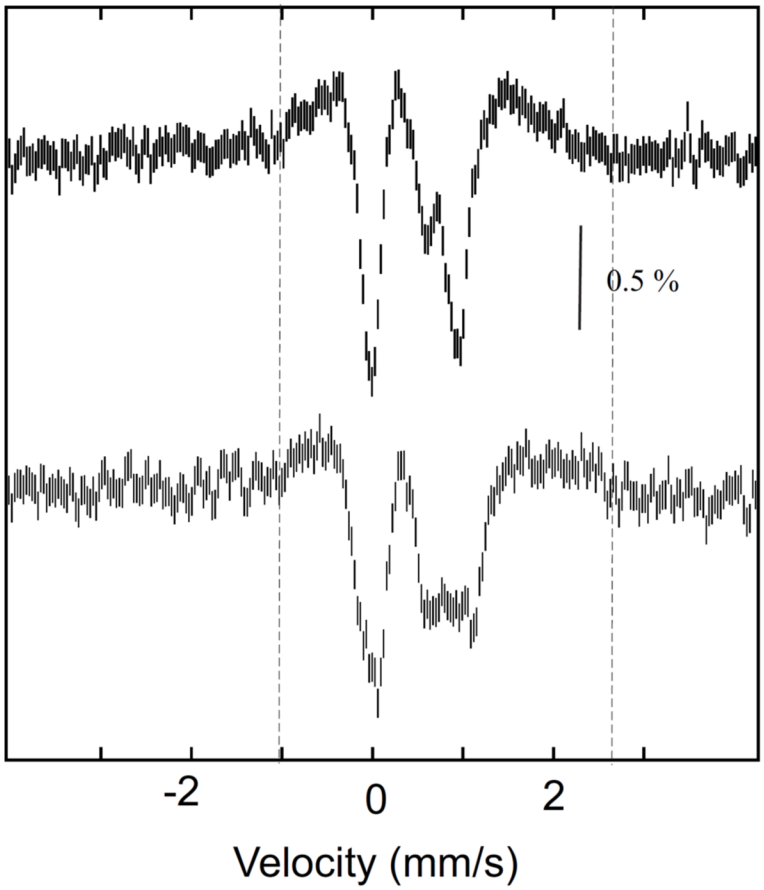

Figure S4. Comparison of [0-53mT] difference spectra of samples containing the $[3Fe\text{-}4S]^0$-like clusters in *Escherichia coli* lipoyl synthase[5] (top) and MiaB (bottom). The vertical dashed lines indicate the width of the magnetically split spectrum.

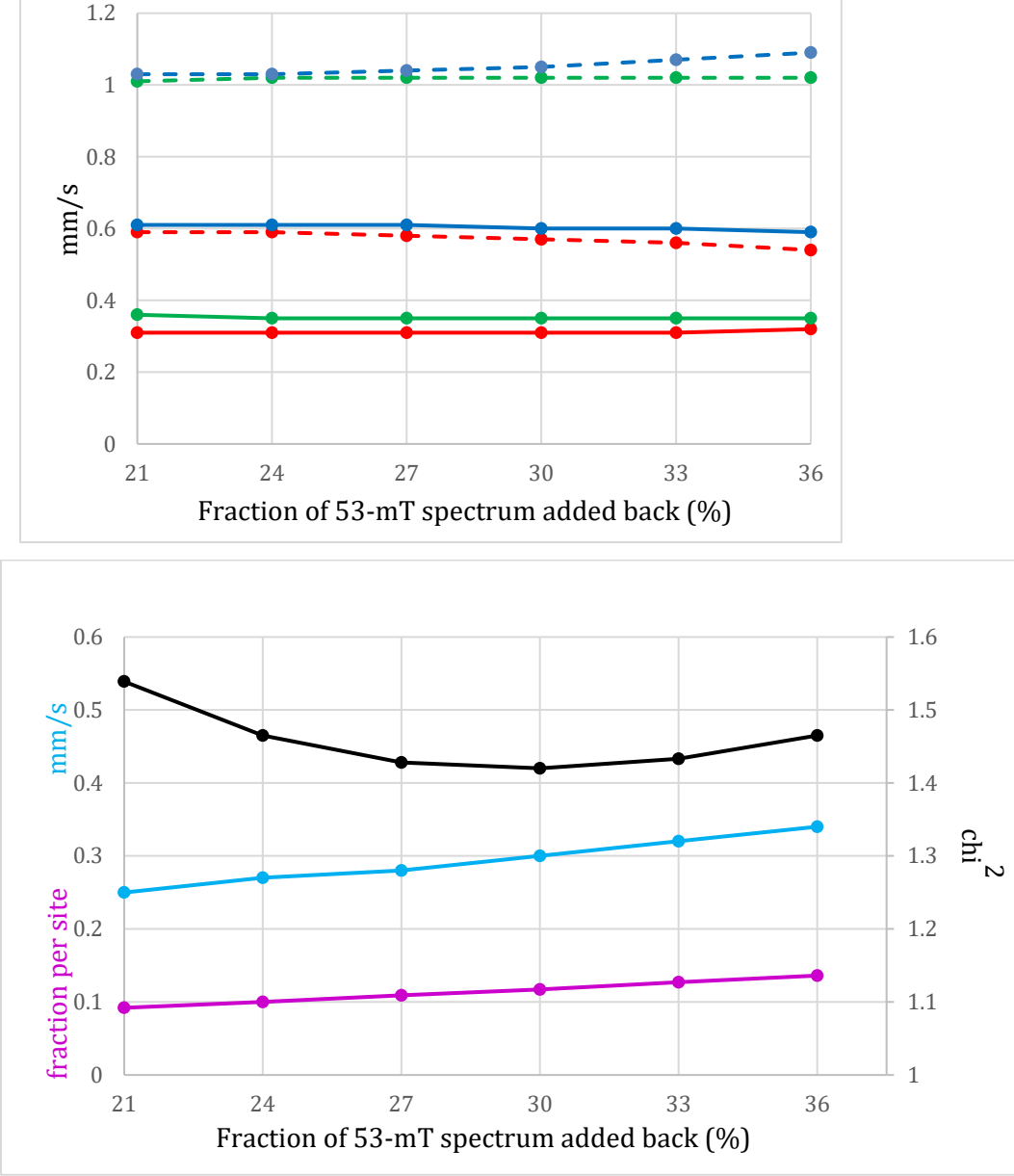

Figure S5. Variation of the Mössbauer parameters obtained from analysis of zero-field reference spectra [δ (top panel, solid lines), ΔE_Q (top panel, dashed lines), line width (bottom panel, cyan line), relative amount (bottom panel, magenta line), and quality of fit, χ^2 (bottom panel, black line) as a function of the relative amount of the simulation of the 53-mT spectrum of the [3Fe-4S]^0-like cluster added back to the [0-53mT] difference spectrum.

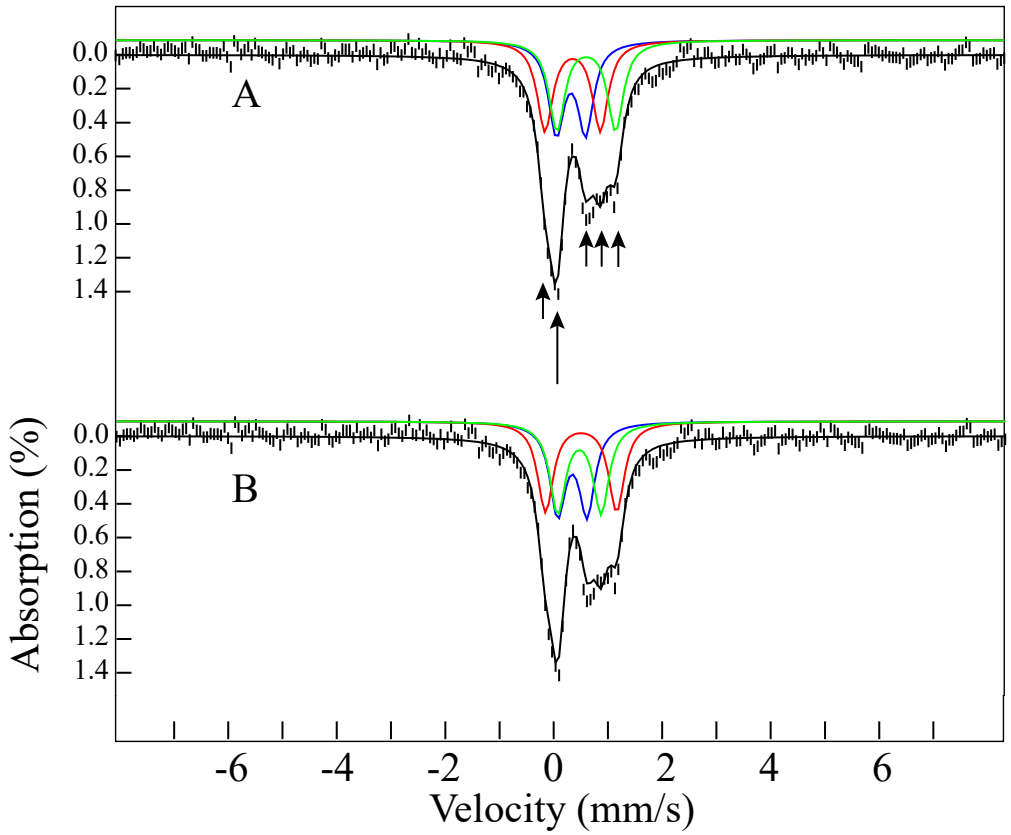

Figure S6. 4.2-K/zero-field Mössbauer reference spectrum of *Bt* MiaB $[3Fe\text{-}4S]^0$-like auxiliary cluster (vertical bars). The spectrum was analyzed with the parameters of solution 1 (**A**) and solution 2 (**B**) from Table 1 of the main manuscript. The blue, red, and green lines are quadrupole doublet simulations associated with sites **1**, **2**, and **3**, respectively. The solid black line overlaid with the experimental spectrum represents the added contribution from the three components.

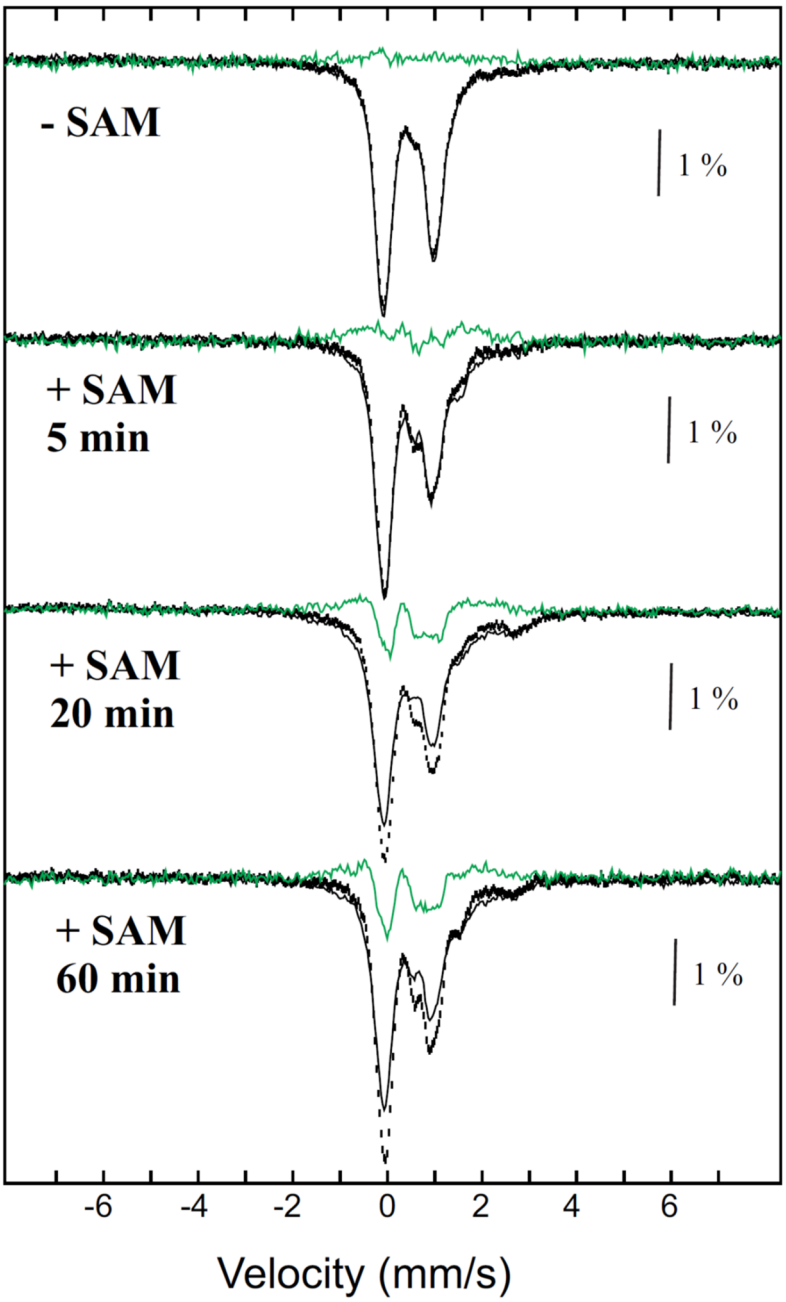

Figure S7. 4.2-K Mössbauer spectra collected in zero applied field (black vertical bars) or a 53-mT magnetic field applied parallel to the γ beam (black lines) of a sample reconstituted *Bt* MiaB WT (top spectra) or samples, where *Bt* MiaB was treated with tRNA substrate and SAM for 5 min, 20 min, or 60 min. The corresponding [0-53mT]-difference spectra are shown as green lines. The samples contain 200 μM *Bt* MiaB reconstituted with ^{57}Fe, 200 μM i^{6}A tRNA^{Phe} and 500 μM SAM.

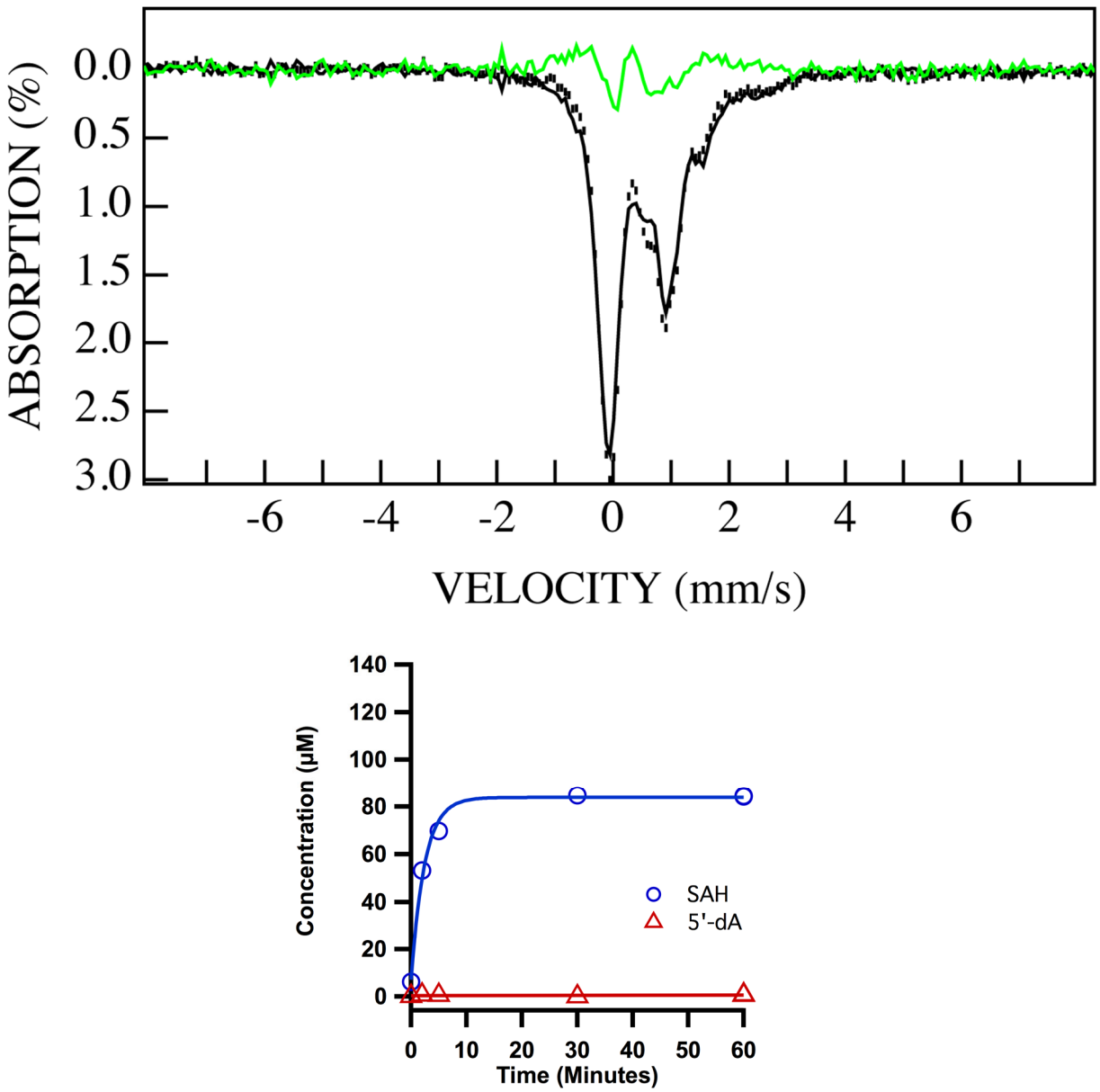

Figure S8. (Top panel) 4.2-K Mössbauer spectra of reconstituted *Bt* MiaB incubated with SAM for 60 min, in the absence of tRNA and low-potential reductant. The spectra recorded in zero-field and field strength of 53 mT are shown as vertical bars and black line, respectively. The [0-53mT] difference spectrum is shown as green line. The amplitude of the difference spectrum is approximately 70% of that of the 20-min sample in the presence of tRNA substrate and SAM. (Lower panel) LC/MS analysis monitoring the formation of SAH (blue circle) and 5′-dA-H (red triangle). The sample contains 200 μM *Bt* MiaB reconstituted with ^{57}Fe and 500 μM SAM.

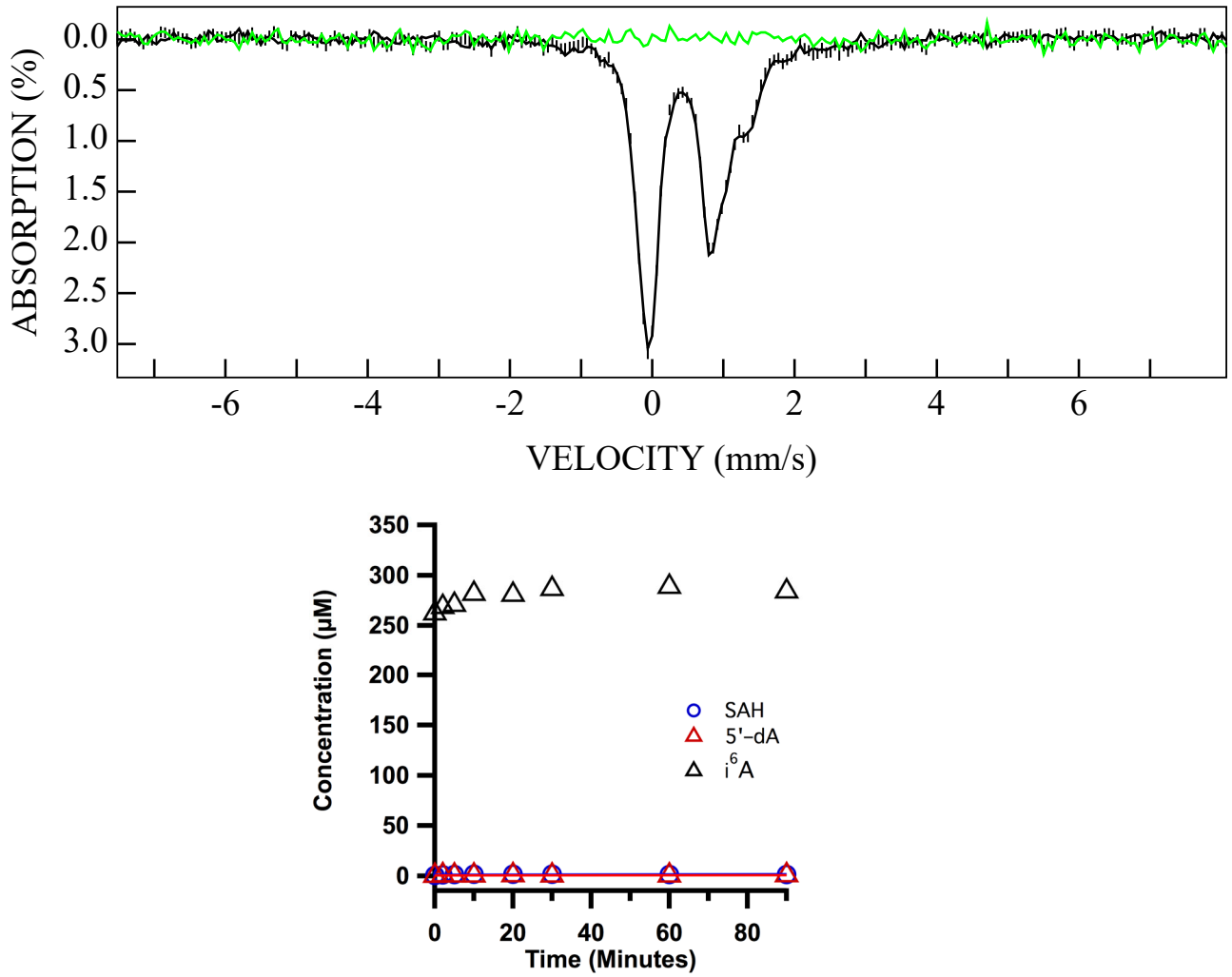

Figure S9. (Top panel) Comparison of zero-field (vertical bars) and 53mT (black line) Mössbauer spectra of reconstituted $^{\Delta Aux}$MiaB (300 μM) incubated with SAM (600 μM) and i^{6}A tRNA (320 μM) for 60 min, in the absence of low-potential reductant. The [0-53mT] difference spectrum is shown as green line. (Lower panel) LC/MS analysis demonstrating that $^{\Delta Aux}$MiaB is incapable of catalyzing the formation of SAH.

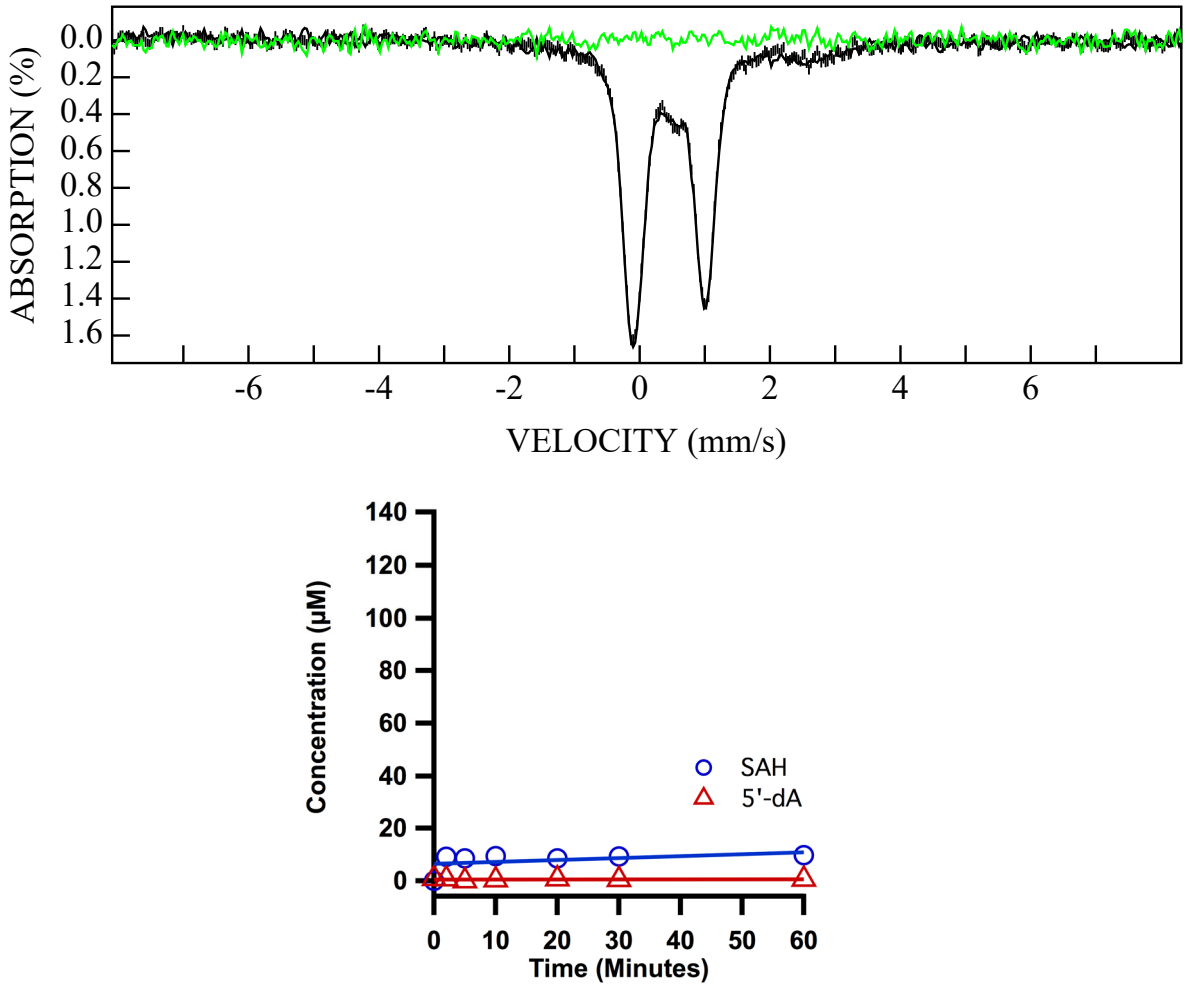

Figure S10. (Top panel) Comparison of zero-field (vertical bars) and 53mT (black line) Mössbauer spectra of reconstituted $^{\Delta RS}$MiaB (300 μM) incubated with SAM (500 μM) and i^{6}A tRNA (200 μM) for 60 min, in the absence of low-potential reductant. The [0-53mT] difference spectrum is shown as green line. (Lower panel) LC/MS analysis demonstrating that $^{\Delta RS}$MiaB is incapable of catalyzing the formation of SAH.

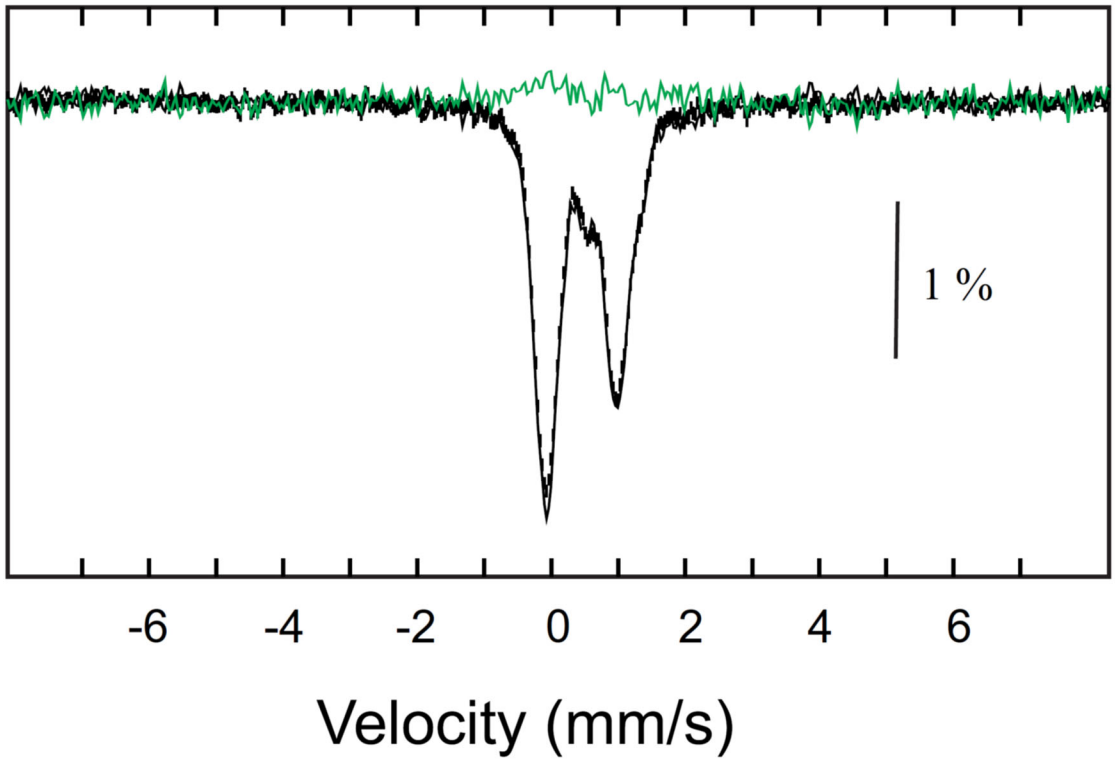

Figure S11. Comparison of 4.2-K/zero-field (vertical bars) and 4.2-K/53-mT (black line) Mössbauer spectra of reconstituted MiaB (300 μM) incubated with i^6A tRNA (200 μM) for 15 min. The [0-53mT] difference spectrum is shown as green line.

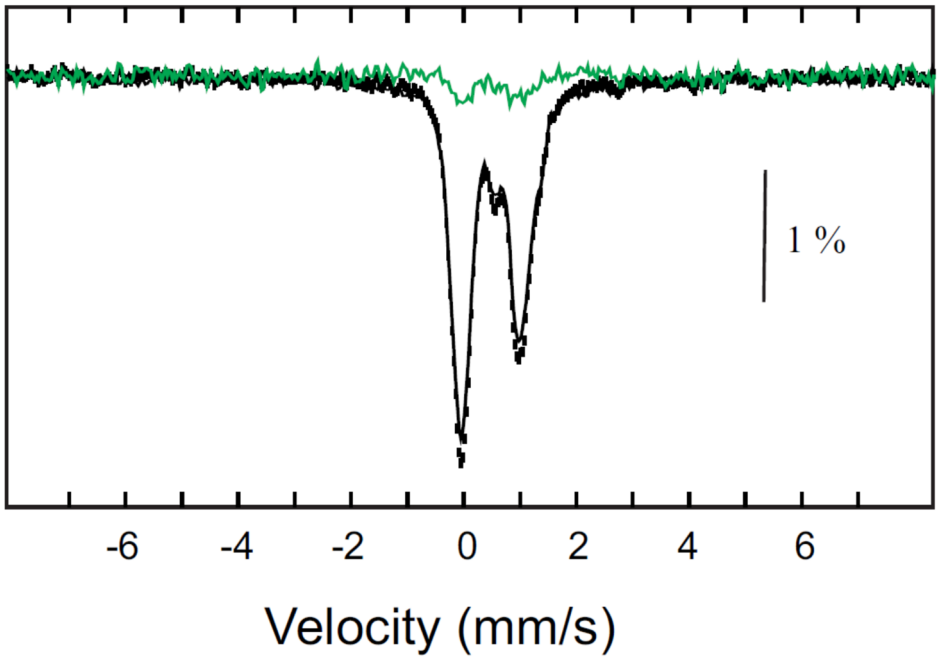

Figure S12. Comparison of 4.2-K/zero-field (vertical bars) and 4.2-K/53-mT (black line) Mössbauer spectra of reconstituted MiaB (200uM) incubated with CH_3SH (1 mM) for 30 min. The [0-53mT] difference spectrum is shown as green line.

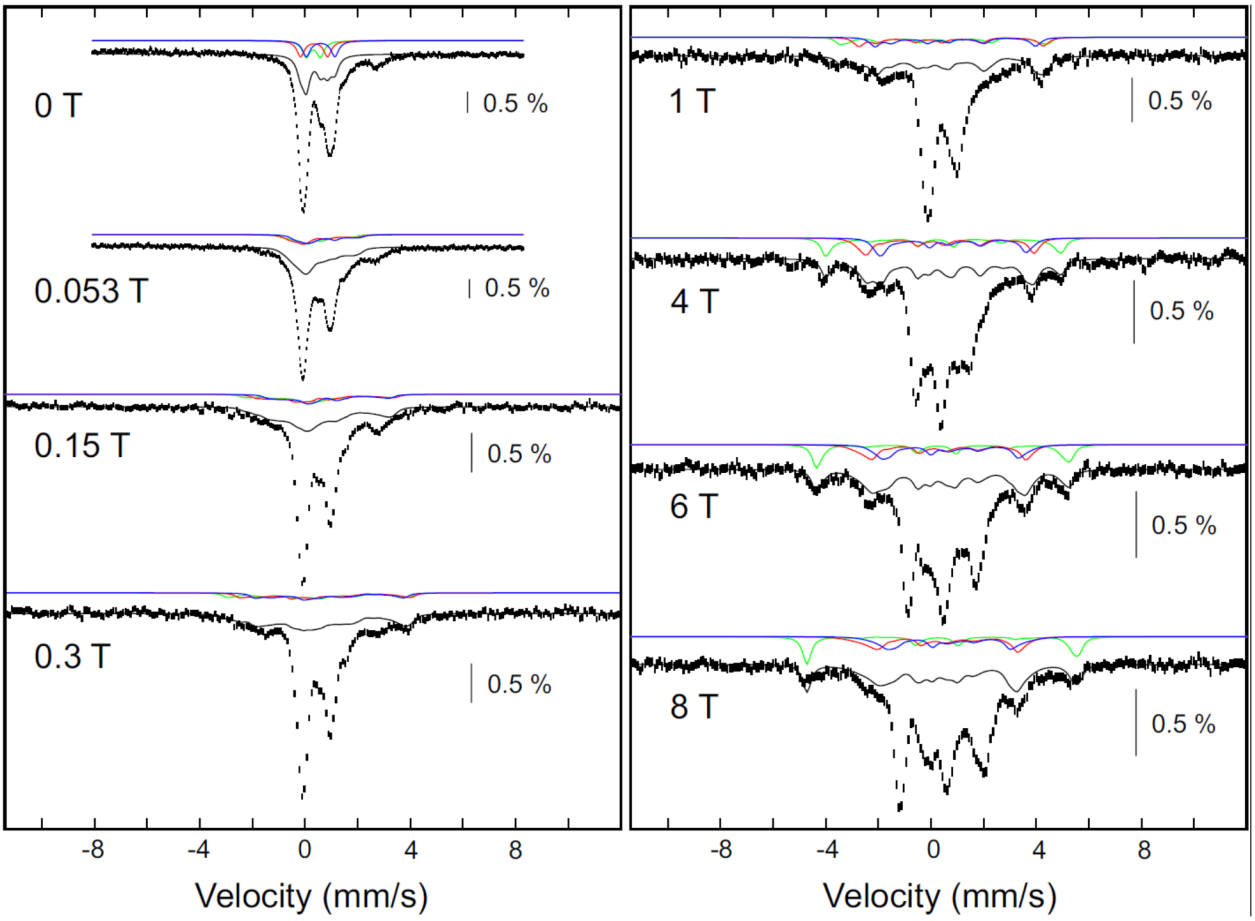

Figure S13A. 4.2-K/variable-field Mössbauer spectra of *Bt* MiaB after incubation with SAM for 20 min. Except for the spectrum recorded in the absence of applied field, all spectra were recorded in magnetic field applied parallel to the γ beam with field strength indicated in the spectra. In all spectra, the experimental data are shown as black vertical bars. The spectral features associated with the $[3Fe\text{-}4S]^0$-like cluster are highlighted by the grey shade. The solid green, red, and blue lines are spin Hamiltonian simulations of the unique Fe^{III} site, the "Fe^{III}-like" site of the MV unit, and the "Fe^{II}-like" site of the MV unit, respectively. The parameters used for spin Hamiltonian simulations are listed in Table 1 of the main manuscript.

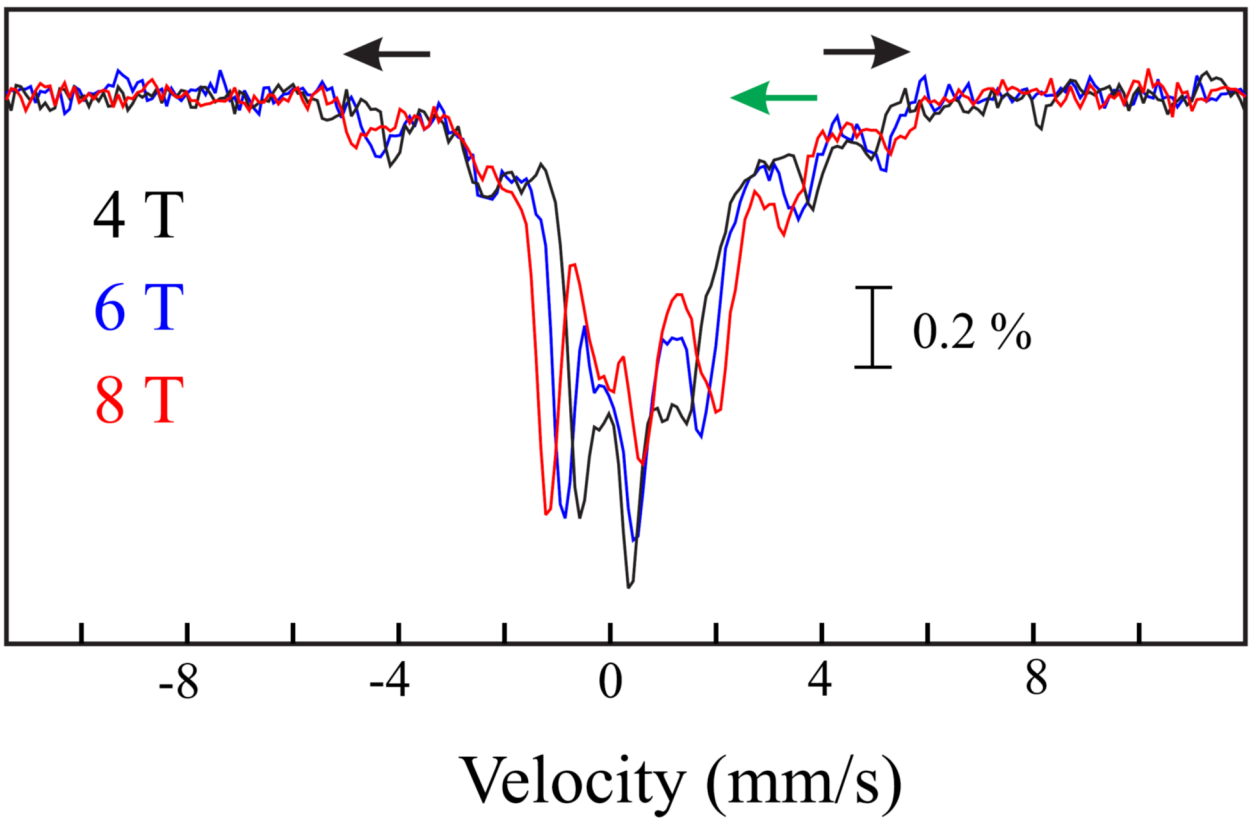

Figure S13B. Comparison of the 4.2-K Mössbauer spectra of *Bt* MiaB after incubation with SAM for 20 min collected in external fields of 4 T (black), 6 T (blue), and 8 T (red). The black arrows indicate the lines of the Fe^{III} site of which the lines move outward with increasing field, while the green arrow indicates the lines of the Fe sites of the MV unit, of which the lines move inward with increasing field.

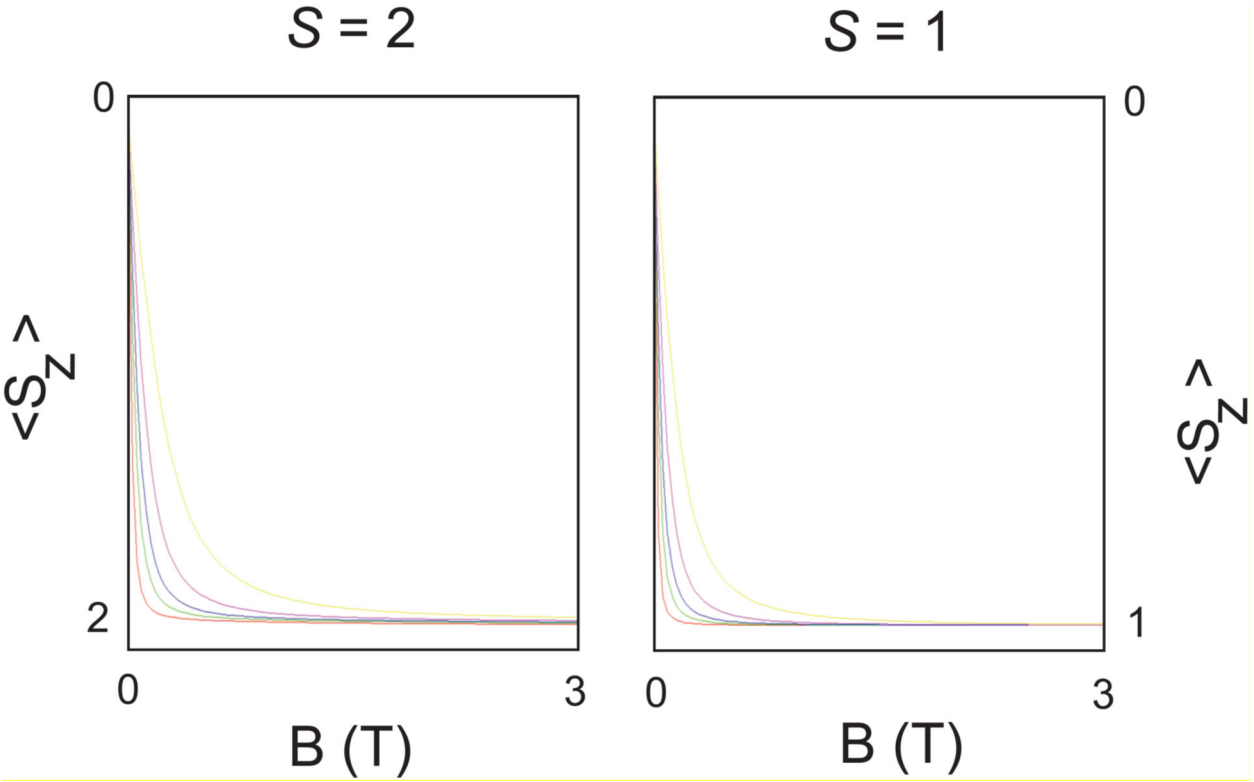

Figure S14 Spin expectation values for an electron spin system with $S = 2$ (left) and $S = 1$ (right), calculated for the electronic ground state with the assumption that the magnetic field is oriented along the z-direction of the zero-field splitting tensor. A rhombicity of $E/D = 0.2$ was assumed for all calculations. The calculations were carried out with values of D of -1 cm^{-1} (red), -2 cm^{-1} (green), -3 cm^{-1} (blue), -5 cm^{-1} (magenta), and -10 cm^{-1} (yellow) for $S = 2$, and with values of D of -0.1 cm^{-1} (red), -0.2 cm^{-1} (green), -0.3 cm^{-1} (blue), -0.5 cm^{-1} (magenta), and -1 cm^{-1} (yellow) for $S = 1$.

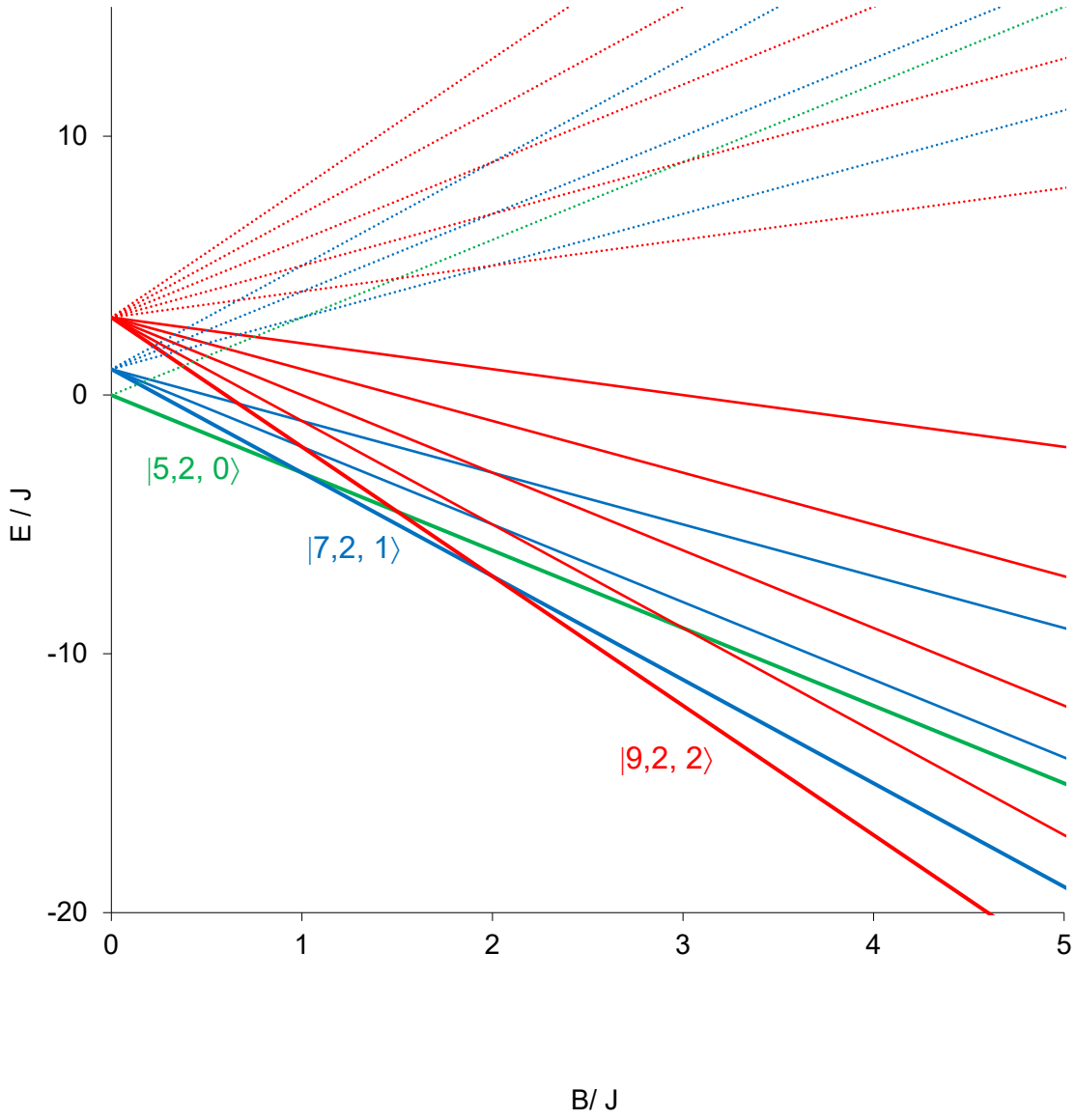

Figure S15A. Energy level diagram according to Equation S2 (or Equation S4 with $J_{mv}/J = 1$). States with $S_{tot} = 0$, $S_{tot} = 1$, and $S_{tot} = 2$ are shown in green, blue, and red. The three possible ground states are indicated with their spin quantum numbers and shown in bolder face.

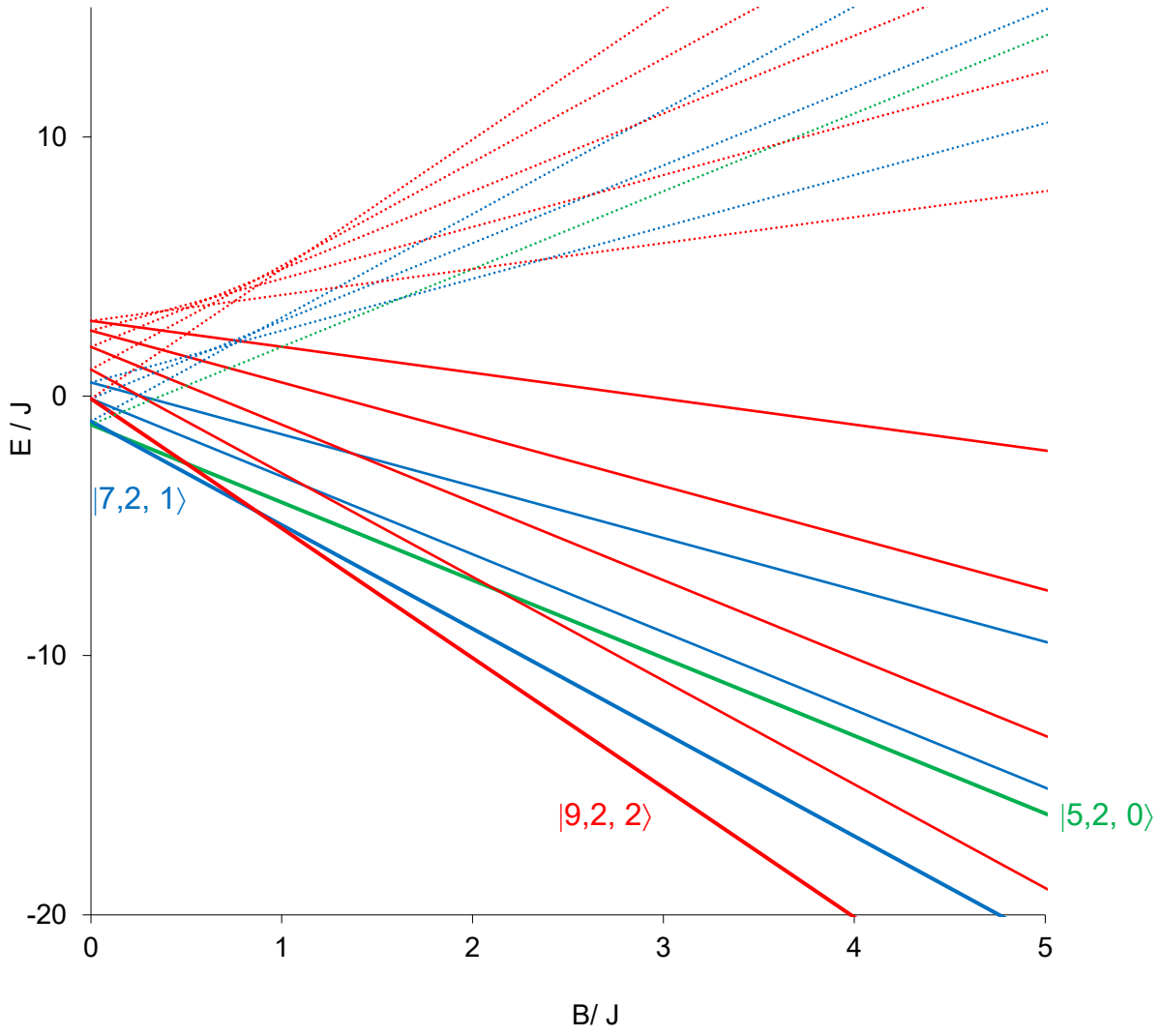

Figure S15B. Energy level diagram according to Equation S4 with $J_{mv}/J = 0.75$. States with $S_{tot} = 0$, $S_{tot} = 1$, and $S_{tot} = 2$ are shown in green, blue, and red. The three possible ground states are indicated with their spin quantum numbers and shown in bolder face.

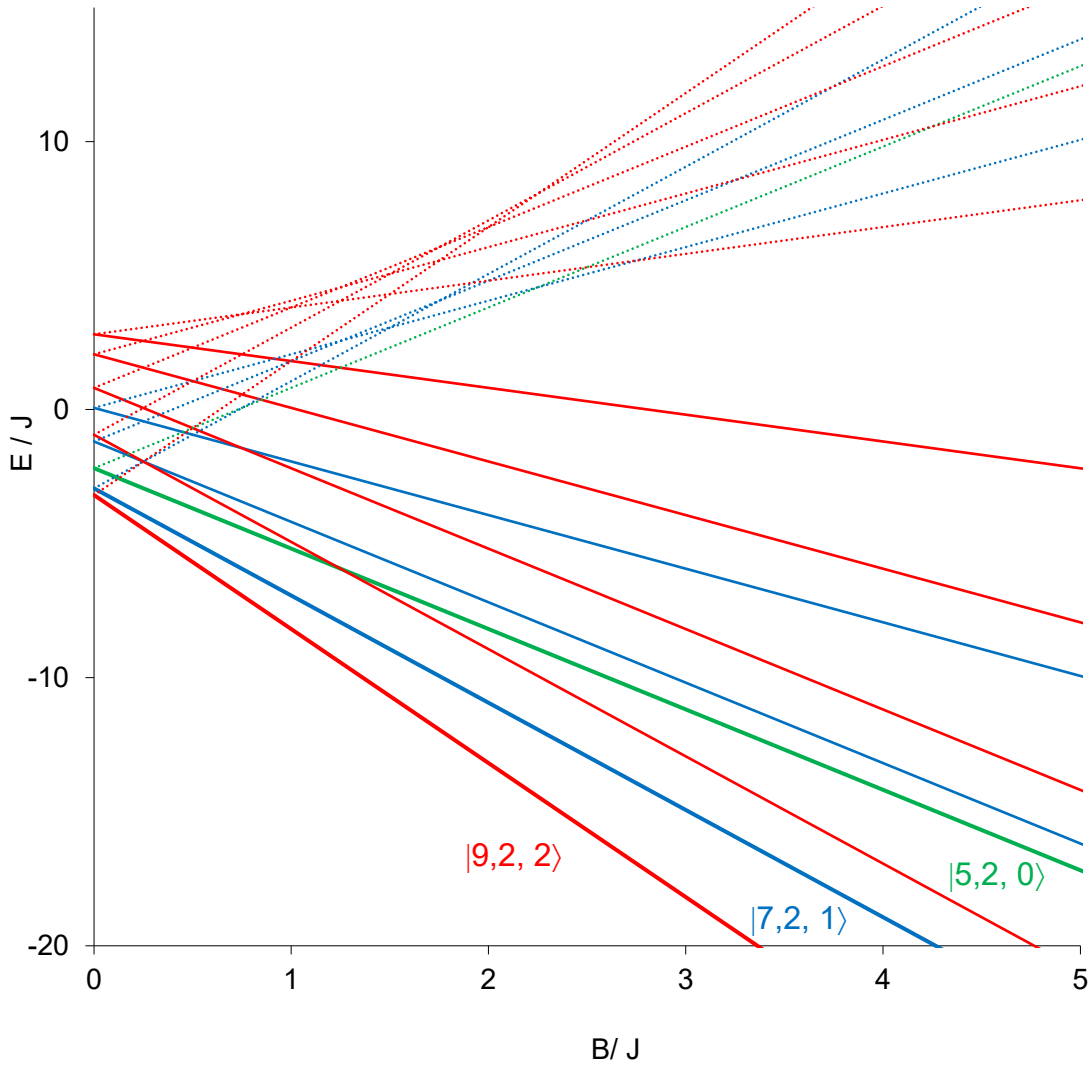

Figure S15C. Energy level diagram according to Equation S4 with $J_{mv}/J = 0.5$. States with S_{tot} = 0, S_{tot} = 1, and S_{tot} = 2 are shown in green, blue, and red. The three possible ground states are indicated with their spin quantum numbers and shown in bolder face.

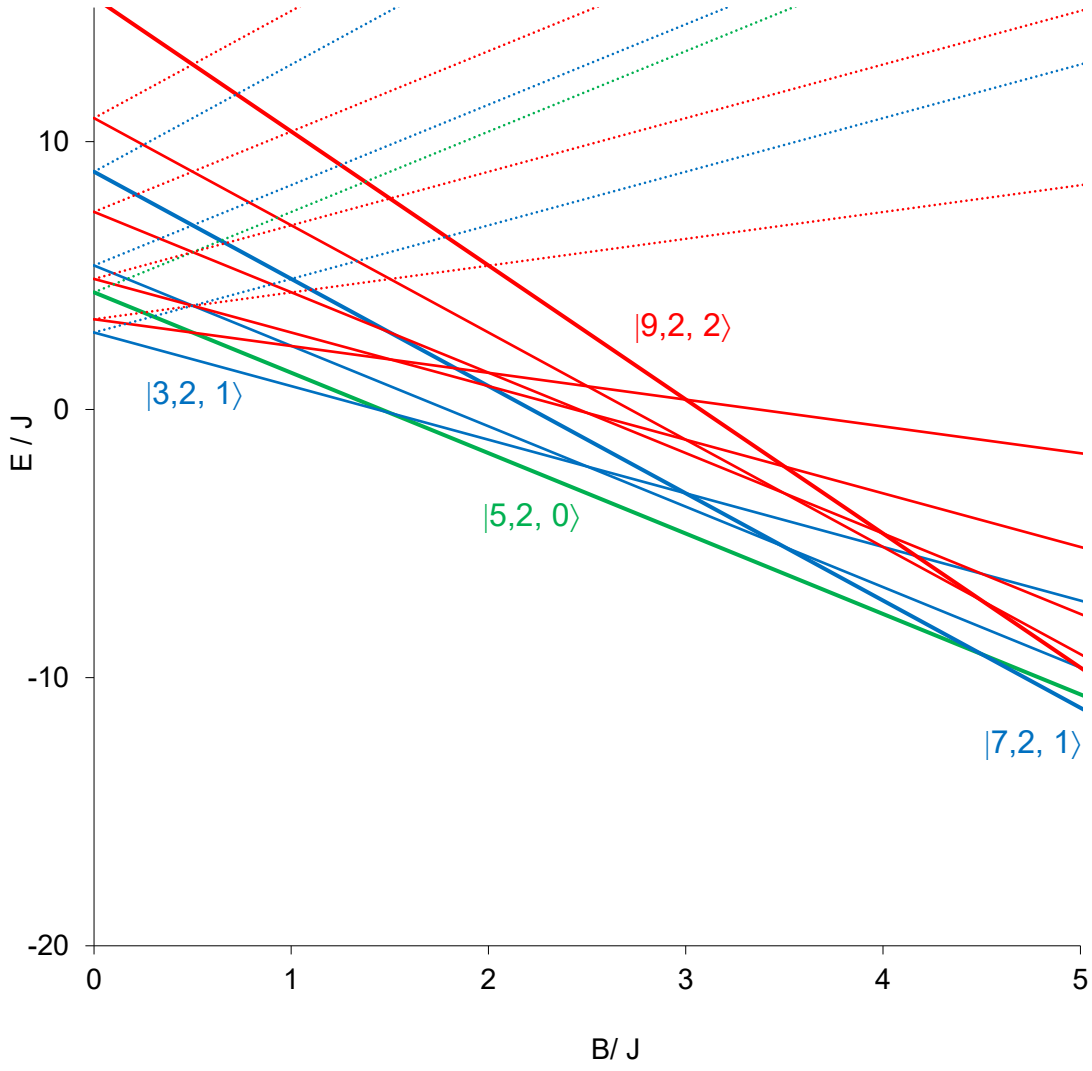

Figure S15D. Energy level diagram according to Equation S4 with $J_{mv}/J = 2$. States with $S_{tot} = 0$, $S_{tot} = 1$, and $S_{tot} = 2$ are shown in green, blue, and red. The three possible ground states are indicated with their spin quantum numbers and shown in bolder face.

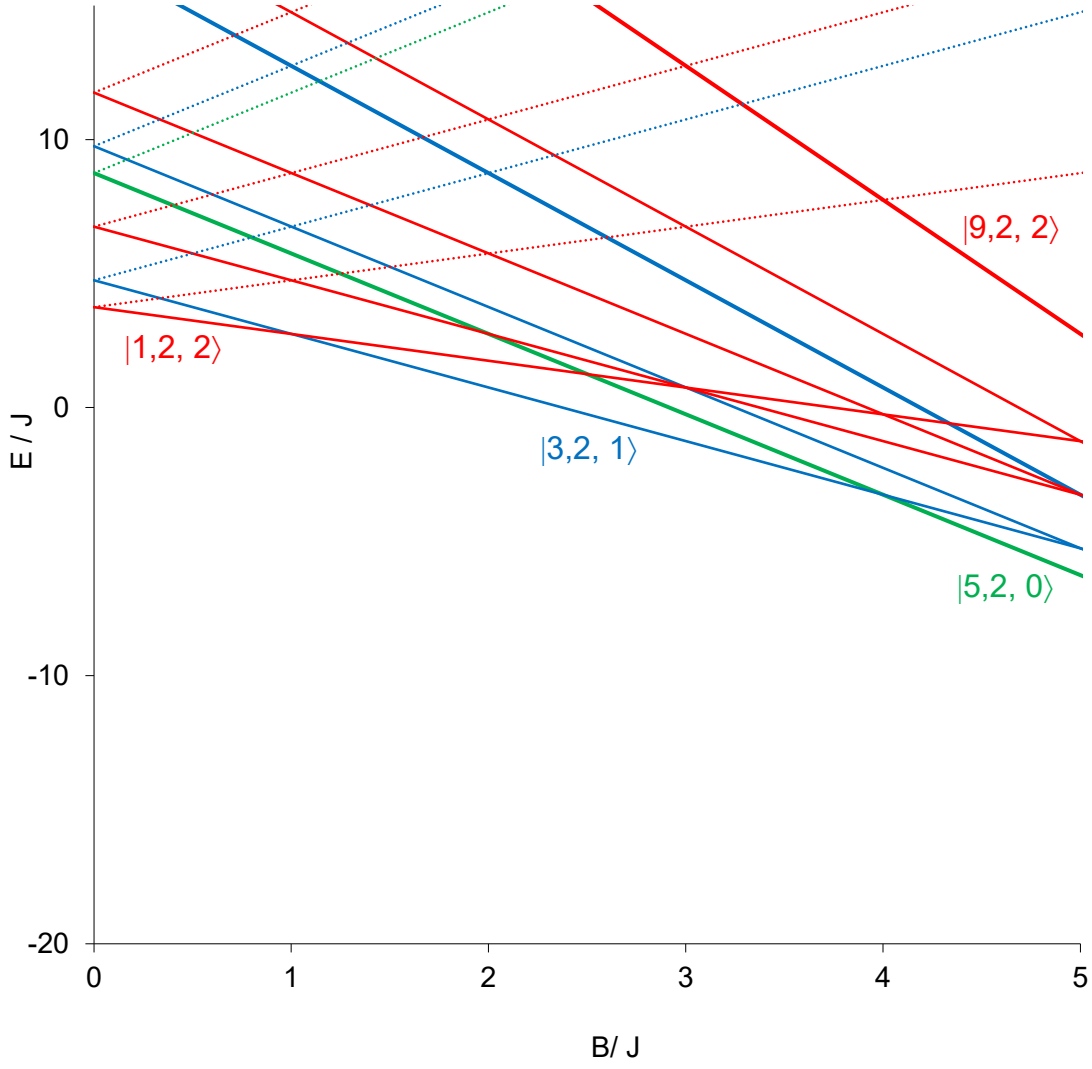

Figure S15E. Energy level diagram according to Equation S4 with $J_{mv}/J = 3$. States with $S_{tot} = 0$, $S_{tot} = 1$, and $S_{tot} = 2$ are shown in green, blue, and red. The three possible ground states are indicated with their spin quantum numbers and shown in bolder face.

References

(1) Landgraf, B. J.; Arcinas, A. J.; Lee, K. H.; Booker, S. J. Identification of an Intermediate Methyl Carrier in the Radical *S*-Adenosylmethionine Methylthiotransferases RimO and MiaB, *J. Am. Chem. Soc.* **2013**, *135*, 15404.

(2) Cicchillo, R. M.; Lee, K. H.; Baleanu-Gogonea, C.; Nesbitt, N. M.; Krebs, C.; Booker, S. J. *Escherichia coli* lipoyl synthase binds two distinct [4Fe-4S] clusters per polypeptide, *Biochemistry* **2004**, *43*, 11770.

(3) Lanz, N. D.; Grove, T. L.; Gogonea, C. B.; Lee, K. H.; Krebs, C.; Booker, S. J.; Hopwood, D. A. RImN and AtsB as Models for the Overproduction and Characterization Radical SAM Proteins, *Natural Product Biosynthesis By Microorganisms and Plants, Pt B* **2012**, *516*, 125.

(4) Lee, K. H.; Saleh, L.; Anton, B. P.; Madinger, C. L.; Benner, J. S.; Iwig, D. F.; Roberts, R. J.; Krebs, C.; Booker, S. J. Characterization of RimO, a New Member of the Methylthiotransferase Subclass of the Radical SAM Superfamily, *Biochemistry* **2009**, *48*, 10162.

(5) Lanz, N. D.; Pandelia, M.-E.; Kakar, E. S.; Lee, K. H.; Krebs, C.; Booker, S. J. Evidence for a Catalytically and Kinetically Competent Enzyme-Substrate Cross-Linked Intermediate in Catalysis by Lipoyl Synthase, *Biochemistry* **2014**, *53*, 4557.

(6) Molle, T.; Clémancey, M.; Latour, J. M.; Kathirvelu, V.; Sicoli, G.; Forouhar, F.; Mulliez, E.; Gambarelli, S.; Atta, M. Unanticipated coordination of tris buffer to the Radical SAM cluster of the RimO methylthiotransferase, *J. Biol. Inorg. Chem.* **2016**, *21*, 549.

(7) Papaefthymiou, V.; Girerd, J. J.; Moura, I.; Moura, J. J. G.; Münck, E. Mössbauer study of *D. gigas* ferredoxin-II and spin-coupling model for the Fe_3S_4 cluster with valence delocalization, *J. Am. Chem. Soc.* **1987**, *109*, 4703.